Composite Structures 270 (2021) 114073

Contents lists available at ScienceDirect

Composite Structures

journal homepage: www.elsevier.com/locate/compstruct

Effects of ply thickness deviation and ply angle misalignment on the surface accuracy of CFRP laminates

Luchao Cheng [a,b], Peng Gong [a,*], Qianglong Wang [a], Meng Zou [c], Yaoyu Zhang [a,b], Zhenyu Liu [a,b]

[a] Changchun Institute of Optics, Fine Mechanics and Physics, Chinese Academy of Sciences, Changchun 130033, China
[b] University of Chinese Academy of Sciences, Beijing 100049, China
[c] Jilin University, Changchun 130012, China

ARTICLE INFO

Keywords:
Ply thickness deviation
Ply angle misalignment
CFRP
Surface accuracy
Zernike polynomial

ABSTRACT

This study examines two factors that affect the surface accuracy of symmetric carbon-fibre-reinforced plastic (CFRP) laminates: ply angle misalignment and ply thickness deviation. First, based on classic laminate theory, theoretical expressions for the effects of these factors are deduced. Then, COMSOL (FEM software) is used to analyse the relationship between these factors and the surface accuracy, and Zernike polynomials are used to fit the surface deformation of the CFRP laminates. It proves that ply angle misalignment and ply thickness deviation can cause astigmatic and power aberrations. Based on the integral constraint method in the form of Lagrangian multipliers, the rigid body displacement problem of the free thermal expansion simulation of CFRP laminates has been solved. Finally, three groups of experimental tests show that ply thickness deviation does occur. A ZYGO interferometer is used to observe the surface accuracy of the laminates, and it shows that astigmatism is the dominant aberration.

1. Introduction

Manufacturing technology and the performance of carbon-fibre-reinforced plastics (CFRP) are constantly improving [1]. CFRP are characterised by high specific stiffness, designability, corrosion resistance, and thermal stability [2–6]. Consequently, there have been many studies on the preparation of carbon-fibre-reinforced composite laminates with high surface accuracy, such as carbon fibre composite reflectors. Such research has examined factors that affect the surface accuracy of laminates to improve their preparation so they can be used for applications in lightweight structural components with highly smooth surfaces. Laminates are manufactured using anisotropic carbon fibre composite prepreg and quasi-isotropic ply angle design. Due to quasi-isotropic ply angle design, laminates can only be quasi-isotropic, rather than isotropic. Many researchers have studied different ply designs [7–9]. These works have shown that even minor agitation during the manufacturing process can have a substantial effect on the surface accuracy.

There are many factors that can affect the surface accuracy of CFRP laminates [10–13], with ply angle misalignment and ply thickness deviation among the most significant. Many researchers have investigated the effects of ply angle misalignment on CFRP laminates. For example, Hinkley examined the effect of ± 2° ply angle misalignments on the elasticity modulus and thermal coefficient of expansion [14]. Vincenti et al. conducted theoretical research on single-layer ply angle misalignment in quasi-isotropic laminates using polar coordinates [15]. Arao et al. showed that, under hot and humid conditions, a ply angle misalignment with a standard deviation of 0.4° caused twisting deformation in symmetrical cross-ply laminates [16,17]. Tanaka et al. studied the thermal deformation sensitivity of a CFRP reflector substrate with respect to the ply angle misalignment [18]. Thompson et al. compared the sensitivity of various lay sequences to the ply angle misalignment [19]. Liu et al. demonstrated that the most effective means of improving the surface accuracy of a space mirror was to reduce the deviation in the alignment angle, followed by decreasing the ply thickness, and optimising the layup sequence [20]. Wilhelmsson et al. investigated the process of measuring ply angle misalignment [21]. Finally, in comparison to the effect of ply thickness deviation on the surface accuracy of CFRP laminates, Steeves and Pellegrino analysed three factors that cause deformation in ultrathin CFRP laminates < 1 mm thick [22]. These factors were ply angle misalignment, ply thickness deviation, and unbalanced temperature

* Corresponding author.
E-mail address: gongpeng0010@163.com (P. Gong).

https://doi.org/10.1016/j.compstruct.2021.114073
Received 22 October 2020; Revised 3 May 2021; Accepted 5 May 2021
Available online 8 May 2021

gradients. They identified the deformation conditions experimentally, and used simulations to show that the even edge thickness of the laminates had the greater effect.

This study aims to examine the effects of ply angle misalignment and ply thickness deviation on the surface accuracy of CFRP laminates. The surface accuracy will be tested with a ZYGO interferometer and the results expressed using aberration fitting with fringe Zernike polynomials. The production of CFRP laminates involves the solidification of epoxy resin, and the moment when the laminate transitions from the glassy state is considered to be the moment of formation [23,24]. The temperature of formation is 120 ℃, so the specimens will be cooled to room temperature. During this process, the CFRP laminates will experience a temperature load and bending deformation will occur under the thermal stress caused by ply angle misalignment and ply thickness deviation. This will affect their surface accuracy. A circular plane laminate with circular symmetry will be considered as the research object in this study to assess the effects of ply angle misalignment and ply thickness deviation on surface accuracy.

The rest of this paper is structured as follows. Section 2 discusses the effects of ply angle misalignment and ply thickness deviation on the surface accuracy of CFRP laminates based on the small-deformation linear classic laminate theory. Section 3 uses COMSOL and Zernike polynomials to fit simulation results obtained using the finite element method (FEM). This is used to analyse the effect of inconsistent ply angles and thicknesses on the surface accuracy of CFRP laminates. In Section 4, three groups of experiments are conducted to examine the effects of ply angle misalignment and ply thickness deviation. Conclusions are provided in Section 5.

2. Theoretical analysis

The effects of ply angle misalignment and ply thickness deviation on the surface accuracy of a circular symmetric CFRP laminate were examined using the small-deformation linear classic laminate theory. Focus on the ply angle misalignment or ply thickness deviation only occurs in a pair of symmetric plies. The elasticity of laminates is described by the equation

$$\begin{Bmatrix} N \\ M \end{Bmatrix} = \begin{bmatrix} A & B \\ B & D \end{bmatrix} \begin{Bmatrix} \varepsilon \\ \kappa \end{Bmatrix} \tag{1}$$

where, N is the in-plane stress, M is the bending moment, A is the in-plane stiffness matrix, B is the stretch–bending coupling stiffness matrix, D is the bending stiffness matrix, ε is the in-plane strain, and κ is the out-plane bending curvature. If the laminate is a symmetric layup, then B = 0. If ply angle misalignment and ply thickness deviation exist, then B ≠ 0 and there will be surface deformation due to the stretch–bending coupling effect.

Based on the thermal expansion theory for composite materials laminates, the in-plane stress and out-plane moment generated by a single-layer ply under a temperature change are given by

$$\begin{Bmatrix} N_x^T \\ N_y^T \\ N_{xy}^T \end{Bmatrix} = \sum_{k=1}^{n} \int_{h_{k-1}}^{h_k} \begin{bmatrix} \sigma_x \\ \sigma_y \\ \sigma_{xy} \end{bmatrix} dz = \sum_{k=1}^{n} \int_{h_{k-1}}^{h_k} \begin{bmatrix} \bar{Q}_{ij} \end{bmatrix} \begin{bmatrix} e_x \\ e_y \\ e_{xy} \end{bmatrix}$$

$$dz = \sum_{k=1}^{n} \begin{bmatrix} \bar{Q}_{11} & \bar{Q}_{12} & \bar{Q}_{16} \\ \bar{Q}_{21} & \bar{Q}_{22} & \bar{Q}_{26} \\ \bar{Q}_{61} & \bar{Q}_{62} & \bar{Q}_{66} \end{bmatrix} \begin{bmatrix} e_x \\ e_y \\ e_{xy} \end{bmatrix} h = \sum_{k=1}^{n} \begin{bmatrix} \bar{Q}_{11} & \bar{Q}_{12} & \bar{Q}_{16} \\ \bar{Q}_{21} & \bar{Q}_{22} & \bar{Q}_{26} \\ \bar{Q}_{61} & \bar{Q}_{62} & \bar{Q}_{66} \end{bmatrix} \begin{bmatrix} \alpha_x \\ \alpha_y \\ \alpha_{xy} \end{bmatrix} h\Delta T$$

$$= \sum_{k=1}^{n} \begin{bmatrix} m^2 & n^2 & -2mn \\ n^2 & m^2 & 2mn \\ mn & -mn & m^2-n^2 \end{bmatrix} \begin{bmatrix} Q_{11} & Q_{12} & 0 \\ Q_{21} & Q_{22} & 0 \\ 0 & 0 & Q_{66} \end{bmatrix} \begin{bmatrix} m^2 & n^2 & mn \\ n^2 & m^2 & -mn \\ -2mn & 2mn & m^2-n^2 \end{bmatrix}$$

$$\begin{bmatrix} m^2 & n^2 & mn \\ n^2 & m^2 & -mn \\ -2mn & 2mn & m^2-n^2 \end{bmatrix}^{-1} \begin{bmatrix} \alpha_L \\ \alpha_T \\ 0 \end{bmatrix} h\Delta T$$

$$= \sum_{k=1}^{n} \begin{bmatrix} m^2 & n^2 & -2mn \\ n^2 & m^2 & 2mn \\ mn & -mn & m^2-n^2 \end{bmatrix} \begin{bmatrix} Q_{11} & Q_{12} & 0 \\ Q_{21} & Q_{22} & 0 \\ 0 & 0 & Q_{66} \end{bmatrix} \begin{bmatrix} \alpha_L \\ \alpha_T \\ 0 \end{bmatrix} \Delta T = \sum_{k=1}^{n} \left[T_\varepsilon^T\right] [Q_{ij}] \begin{bmatrix} \alpha_L \\ \alpha_T \\ 0 \end{bmatrix} h\Delta T \tag{2}$$

and

$$\begin{bmatrix} M_x^T \\ M_y^T \\ M_{xy}^T \end{bmatrix} = \sum_{k=1}^{n} \int_{h_{k-1}}^{h_k} \begin{bmatrix} \sigma_x \\ \sigma_y \\ \sigma_{xy} \end{bmatrix} z_k dz = \sum_{k=1}^{n} \int_{h_{k-1}}^{h_k} \begin{bmatrix} \bar{Q}_{ij} \end{bmatrix} \begin{bmatrix} e_x \\ e_y \\ e_{xy} \end{bmatrix}$$

$$z_k dz = \sum_{k=1}^{n} \begin{bmatrix} \bar{Q}_{ij} \end{bmatrix} \begin{bmatrix} e_x \\ e_y \\ e_{xy} \end{bmatrix} h z_k = \sum_{k=1}^{n} \begin{bmatrix} \bar{Q}_{11} & \bar{Q}_{12} & \bar{Q}_{16} \\ \bar{Q}_{21} & \bar{Q}_{22} & \bar{Q}_{26} \\ \bar{Q}_{61} & \bar{Q}_{62} & \bar{Q}_{66} \end{bmatrix} \begin{bmatrix} \alpha_x \\ \alpha_y \\ \alpha_{xy} \end{bmatrix} h z_k \Delta T$$

$$= \sum_{k=1}^{n} \begin{bmatrix} m^2 & n^2 & -2mn \\ n^2 & m^2 & 2mn \\ mn & -mn & m^2-n^2 \end{bmatrix} \begin{bmatrix} Q_{11} & Q_{12} & 0 \\ Q_{21} & Q_{22} & 0 \\ 0 & 0 & Q_{66} \end{bmatrix}$$

$$\begin{bmatrix} m^2 & n^2 & mn \\ n^2 & m^2 & -mn \\ -2mn & 2mn & m^2-n^2 \end{bmatrix} \begin{bmatrix} m^2 & n^2 & mn \\ n^2 & m^2 & -mn \\ -2mn & 2mn & m^2-n^2 \end{bmatrix}^{-1} \begin{bmatrix} \alpha_L \\ \alpha_T \\ 0 \end{bmatrix} h z_k \Delta T$$

$$= \sum_{k=1}^{n} \begin{bmatrix} m^2 & n^2 & -2mn \\ n^2 & m^2 & 2mn \\ mn & -mn & m^2-n^2 \end{bmatrix} \begin{bmatrix} Q_{11} & Q_{12} & 0 \\ Q_{21} & Q_{22} & 0 \\ 0 & 0 & Q_{66} \end{bmatrix} \begin{bmatrix} \alpha_L \\ \alpha_T \\ 0 \end{bmatrix}$$

$$h z_k \Delta T = \sum_{k=1}^{n} \left[T_\varepsilon^T\right] [Q_{ij}] \begin{bmatrix} \alpha_L \\ \alpha_T \\ 0 \end{bmatrix} h z_k \Delta T \tag{3}$$

respectively. Here, x and y denote orthogonal directions in the plane of the laminate; T_ε is the transformation matrix in relation to the ply angles; Q_{ij} is an on-axis modulus component (i, j = 1, 2, 6); $\bar{Q}_{ij}$ is the result of the transformation of Q_{ij} ; α_L and α_T are thermal expansion coefficients of the ply in the horizontal and vertical directions of the fibre, respectively; h is the thickness of a single lay; ΔT is the temperature difference; and z_k is the distance from the edge of the laminate to the mid-plane.

The thermal vector relationship for inner stress in certain ply of the laminate, equivalent to a specified coordinate direction at an angle θ from the direction of fibre, is given by

$$\begin{bmatrix} N_x \\ N_y \\ N_{xy} \end{bmatrix} = \left[T_\varepsilon^T\right] [Q_{ij}] \begin{bmatrix} \alpha_L \\ \alpha_T \\ 0 \end{bmatrix} h\Delta T \Rightarrow \begin{cases} N_x = [m^2(\alpha_L Q_{11} + \alpha_T Q_{12}) + n^2(\alpha_L Q_{12} + \alpha_T Q_{22})]h\Delta T \\ N_y = [n^2(\alpha_L Q_{11} + \alpha_T Q_{12}) + m^2(\alpha_L Q_{12} + \alpha_T Q_{22})]h\Delta T \\ N_{xy} = [mn(\alpha_L Q_{11} + \alpha_T Q_{12} - \alpha_L Q_{12} + \alpha_T Q_{22})]h\Delta T \end{cases}$$

$$\begin{cases} N_x = \frac{1}{2}h(E\cos 2\theta + F)\Delta T \\ N_y = \frac{1}{2}h(-E\cos 2\theta + F)\Delta T \\ N_{xy} = \frac{1}{2}hE\Delta T \sin 2\theta \end{cases} \tag{4}$$

where,

$$\begin{cases} \mathrm{m} = \cos\theta \\ \mathrm{n} = \sin\theta \\ E = \alpha_L Q_{11} + \alpha_T Q_{12} - \alpha_L Q_{12} - \alpha_T Q_{22} \\ F = \alpha_L Q_{11} + \alpha_T Q_{12} + \alpha_L Q_{12} + \alpha_T Q_{22} \end{cases} \tag{5}$$

and h is the thickness of a single layer. E and F are constants related to the properties of the material. Therefore, it can be seen the equivalent thermal stresses are functions of just the ply angle and single-layer ply thickness from Eq. (4) and (5).

2.1. Theoretical analysis of surface deformation caused by ply angle misalignment

Ply angle misalignment is unavoidable during the CFRP laminate manufacturing process. If ply angle misalignment only occurs in a pair

of symmetric plies, an agitation $\Delta\theta$ may be assumed. From Eq. (4), the equivalent thermal stress vector difference and torque difference of the mid-plane are

$$\begin{cases} \Delta N_x = [E(\cos 2(\theta+\Delta\theta)-\cos 2\theta)]\frac{h}{2}\Delta T \\ \Delta N_y = [-E(\cos 2(\theta+\Delta\theta)-\cos 2\theta)]\frac{h}{2}\Delta T \end{cases} \quad (6)$$

and

$$\begin{cases} \Delta M_x = [E(\cos 2(\theta+\Delta\theta)-\cos 2\theta)]\frac{h}{2}z_k\Delta T \\ \Delta M_y = [-E(\cos 2(\theta+\Delta\theta)-\cos 2\theta)]\frac{h}{2}z_k\Delta T \end{cases} \quad (7)$$

respectively. This shows that the stretch–bending moments about the symmetric mid-plane of the laminate occur in opposite directions along a given axis, that is ΔM_x = -ΔM_y. Thus, the moments will be greatest if this axis is aligned with the tow where ply angle misalignment exists (the main stress direction). The deformation of CFRP laminates caused by moments with opposite directions is approximately saddle-shaped. Fitting with fringe Zernike polynomials shows that the deformation is an astigmatic aberration.

In this study, the first nine substrates of fringe Zernike polynomials and their corresponding coefficients were used to fit the surface. The focus was on the corresponding fitting coefficient using the least minimum square method. The deformations mainly corresponded to item 4 (power) and items 5 and 6 (astigmatism) in the fringe Zernike polynomials, called the power and astigmatism aberrations, respectively. These are shown in Table 1, where r is the radius and θ is the angle [25].

2.2. Theoretical analysis of surface deformation caused by ply thickness deviation

Based on the theory of small-deformation linear elastic classic laminates, when ply thickness deviation only occurs in a pair of symmetric plies of a symmetrical laminate, the equivalent thermal vector and thermal torque in any direction in the laminate are given by

$$\begin{cases} \Delta N_x = \frac{1}{2}\Delta h(E\cos 2\theta_k + F) \\ \Delta N_y = \frac{1}{2}\Delta h(-E\cos 2\theta_k + F) \end{cases} \quad (8)$$

and

$$\begin{cases} \Delta M_x = \frac{1}{2}\Delta h(E\cos 2\theta_k + F)z_k \\ \Delta M_y = \frac{1}{2}\Delta h(-E\cos 2\theta_k + F)z_k \end{cases} \quad (9)$$

respectively. Δh is the ply thickness deviation only occurs in a pair of symmetric plies of a symmetrical laminate.

The principal stress for the in-plane force in the ply is orientated horizontally and perpendicular to the direction of the tow. Therefore, when the middle plane coordinate of the laminate coincides with principal stress direction in the ply with the thickness deviation, the equivalent thermal stress and moment have maximum and minimum values, respectively. From Eq. (8) and (9), the positive and negative values of the moment are determined by the positive and negative values of E and F. The mechanical properties of the material adopted in this study is listed in Table 2. The calculated results are E $\approx -429770.45 < 0$, F $\approx 260732.36 > 0$. Substituting E, F, and $\theta = 0^\circ$ into Eq. (9) gives $\Delta M_x < 0$ and $\Delta M_y > 0$, which have different absolute values and opposite signs. Next, ΔM_y may be separated into ΔM_{y1} and ΔM_{y2}, where $|\Delta M_{y1}| = |\Delta M_x|$. Similarly, ΔM_{y1} and ΔM_x have the same torque but opposite signs, which will cause saddle-shaped deformation in laminates. It turns out that this is an astigmatic aberration fit with Zernike polynomials. Moreover, ΔM_{y2} will cause curved deformation in laminates, which corresponds to other aberrations with a smaller magnitude than the astigmatism in the Zernike fit.

Table 1
Fringe Zernike polynomials.

Number	4	5	6
Fringe Zernike polynomials	$2r^2$-1	$r^2\cos(2\theta)$	$r^2\sin(2\theta)$

3. Simulation analysis

In this section, the effects of ply angle misalignment and ply thickness deviation on the surface accuracy are verified numerically through simulation analyses. Focus on the relationships between ply angle misalignment or ply thickness deviation and power or astigmatic aberration. A circular plane laminate (Ply angle is $[90\text{–}45\ 45\ 0]_{2s}$, 70 mm in diameter and thickness is 1.6 mm) with circular symmetry will be considered as the research object of simulation in section 3 and experiment in section 4.

A simulated geometrical model, 70 mm in diameter and 1.6 mm in thickness, was constructed using COMSOL for mesh division of finite elements, as shown in Fig. 1. Linear Lagrangian hexahedral element are used. Based on Eq. (2) and (3), thermal loading due to temperature difference of 100 ℃ has been applied by COMSOL script. In the simulation, the first nine items of the Zernike polynomial were adopted for deformation fitting.

Preparation technology of the laminate is vacuum bag technology in this study (details of preparation technology in section 4.1). The top and bottom of the laminate are pressed by two pieces of glass–ceramic mold in vacuum bag. It can be found that the simulation of this section is a free expansion simulation through preparation technology of the laminate. The rigid body displacement problem of the free thermal expansion simulation is solved as follows.

According to the FEM, the total potential energy of discrete type materials in elastic mechanics can be expressed as

$$\Pi = \frac{1}{2}U^TKU - U^TF \quad (10)$$

where, Π is the total discrete type potential energy, **U** is the overall displacement calculated using the FEM, **F** is the external load, and **K** is the stiffness matrix. This study is focussed on the free thermal expansion of laminates. Rigid body displacement occurs in the geometric model due to the lack of constraints on the finite element calculations. To address this, two Lagrangian multiplier integral constraints are introduced for the x- and y-directions across the whole domain. The displacement in three directions at the centre of the bottom surface is fixed. These conditions can be expressed as

$$\begin{aligned} &\Pi = \tfrac{1}{2}U^TKU - U^TF \\ &\textstyle\int_\Omega l_u U d\Omega = 0 \\ &\textstyle\int_\Omega l_v U d\Omega = 0 \end{aligned} \quad (11)$$

where, l_u is a row vector with 1 in the locations corresponding to the x-direction in **U** and 0 elsewhere; and l_v is a column vector corresponding to the y-direction. The Lagrangian multiplier constraints

Table 2
Engineering elastic constants of T700 CFRP Prepreg.

Material	E_L [GPa]	E_T [GPa]	ν_L	ν_T	G_{LT}	α_L	α_T
T700	134	9.42	0.28	0.02	6.5	−1.35e-6	36.83e-6

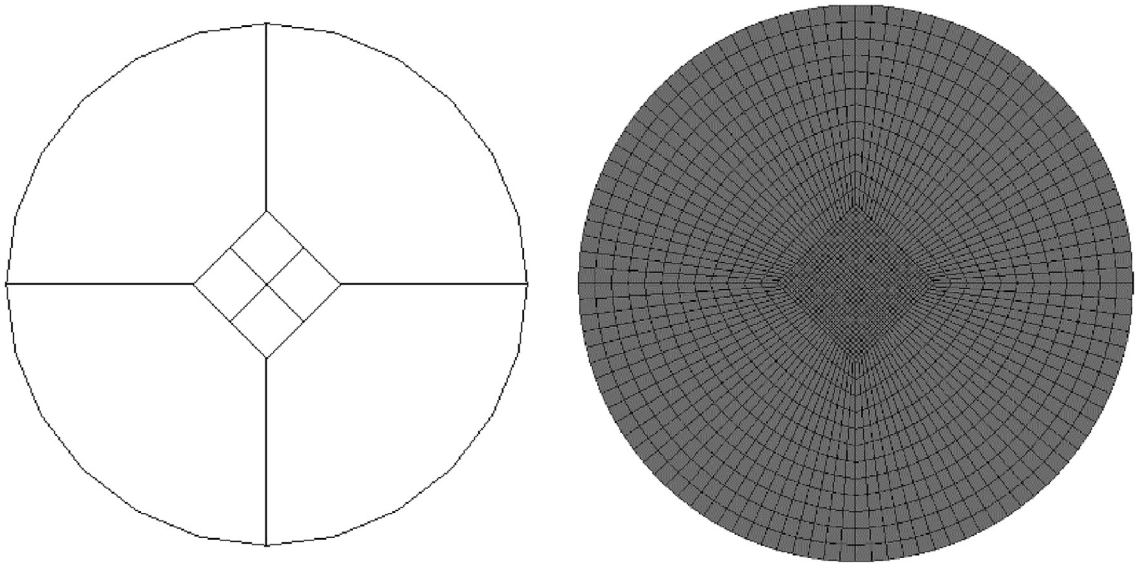

Fig. 1. Simulated geometrical model and mesh division of finite elements obtained using COMSOL.

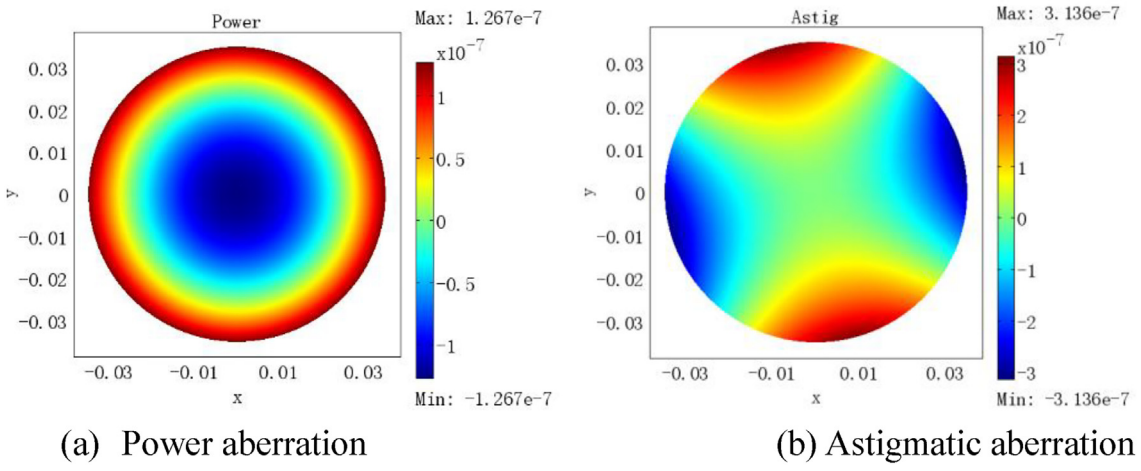

Fig. 2. Simulation of the power and astigmatic aberrations at various ply angle misalignments.

address the problem of random rigid body displacement by restricting the position of the whole domain. When the Lagrangian multipliers are introduced, the total potential energy can be expressed as follows.

$$\Pi^* = \frac{1}{2}U^T KU - U^T F + \lambda_1 \int_\Omega l_u U d\Omega + \lambda_2 \int_\Omega l_v U d\Omega \tag{12}$$

Calculating the variation about U and setting it to zero gives the following:

$$\begin{aligned} &\tfrac{\partial \Pi^*}{\partial U} = KU - F + \lambda_1 l_u|_\Omega + \lambda_2 l_v|_\Omega = 0 \\ &KU = F - \lambda_1 l_u|_\Omega - \lambda_2 l_v|_\Omega \\ &KU = -\lambda_1 l_u|_\Omega - \lambda_2 l_v|_\Omega \end{aligned} \tag{13}$$

From this, the two items on the right can be disposed as two body loads in the x- and y-directions of the domain, and corresponding values of λ_1 and λ_2 are obtained. The two Lagrangian multipliers, solved using the 'global equation' in COMSOL, are added to the corresponding body loads so that the finite element calculation can be completed without random rigid body displacement.

3.1. Simulation analysis of the relationship between ply angle misalignment and astigmatic aberration

Twenty groups of random number sequences were generated using the Monte Carlo method. Based on the preparation of CFRP laminates, the standard deviation 0.4 and the mean value 0 of twenty groups of random number sequences were selected for the ply angle misalignment. During the finite element simulation, these were superimposed on the ply angle to simulate misalignment. Finally, the astigmatisms and power aberrations at various ply angle misalignments were obtained from the simulation of the CFRP laminate surface accuracy, as shown in Figs. 2 and 3, respectively.

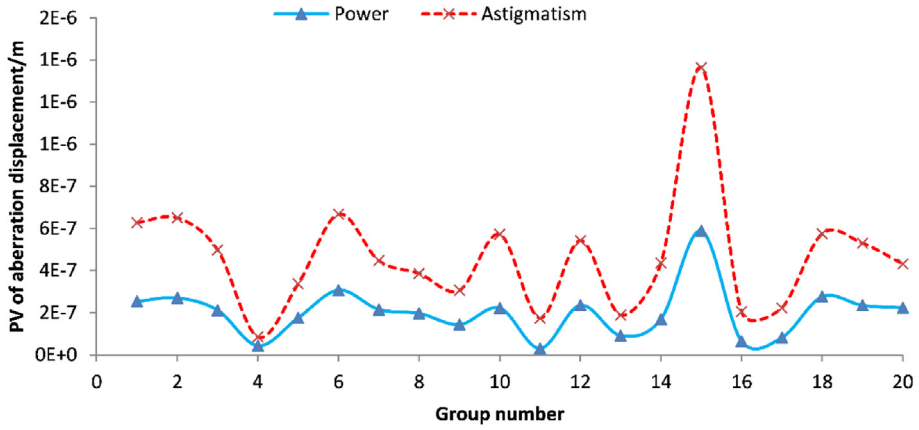

Fig. 3. Simulated results for power and astigmatic aberrations.

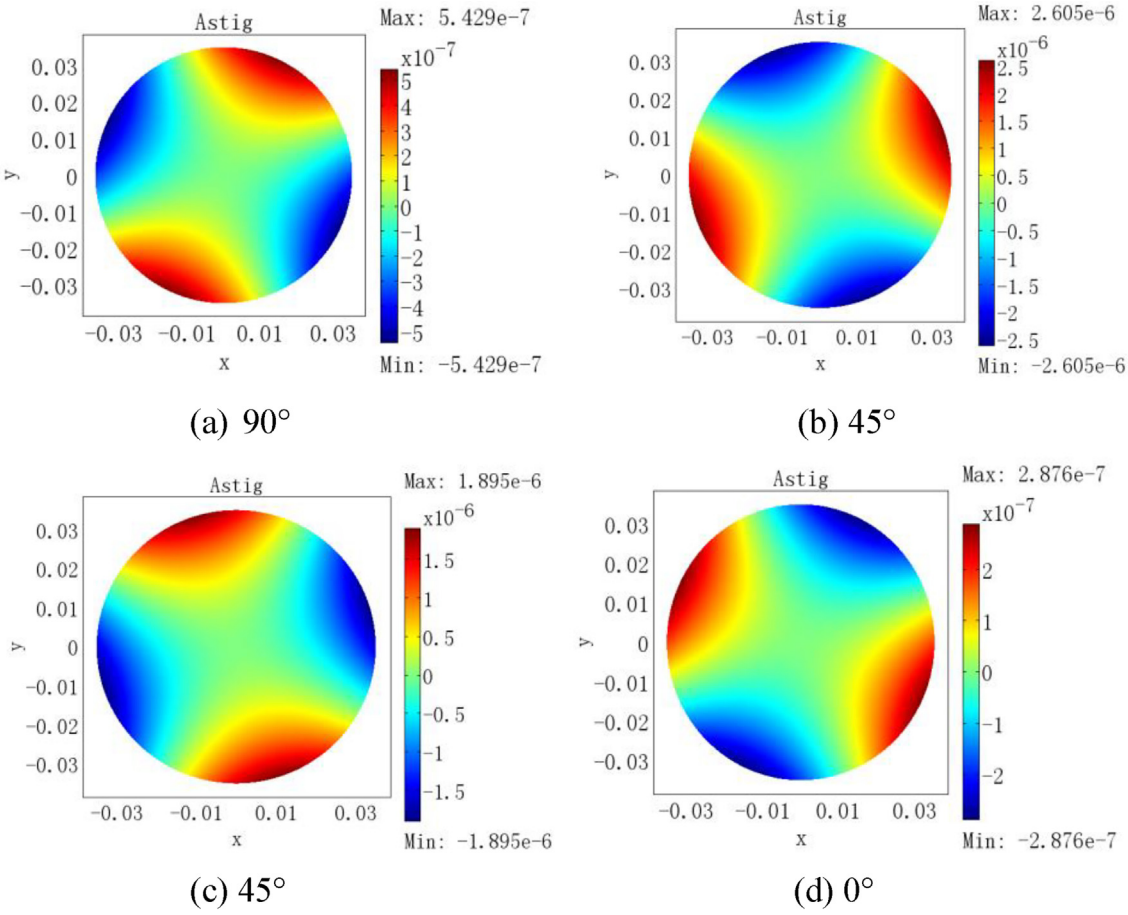

Fig. 4. Simulated astigmatic aberrations with a constant ply thickness deviation applied at different angles.

Fig. 3 shows that the power and astigmatic aberrations experienced similar variations. Moreover, ply angle misalignment mainly causes astigmatic aberrations with magnitudes of the order 10^{-7}–10^{-6}.

3.2. Simulation analysis for relations between ply thickness deviation and power and astigmatic aberrations

3.2.1. Relationship between ply thickness deviation and lay–up angle

The total thickness of the laminate was fixed at 1.6 mm, and the thickness deviation of a pair of symmetric plies was changed from 0 to 20 μm at 1 μm intervals. That is, there were 20 groups of thickness deviation simulations for every pair of symmetric plies. There were eight pairs of symmetric plies, so there were 160 groups in total. The simulation results, presented in Fig. 4, show that the astigmatic aberration distribution is related to the direction of the misaligned ply (i.e., the layup angle). Opposite results were obtained for 0° and 90°, and 45° and −45°, respectively. Fig. 5 shows that the value of the astigmatic aberration is linearly dependant on the ply thickness deviation of the same ply angle. Furthermore, for the same ply thickness deviation, the sensitivity of different ply angles varies from strong

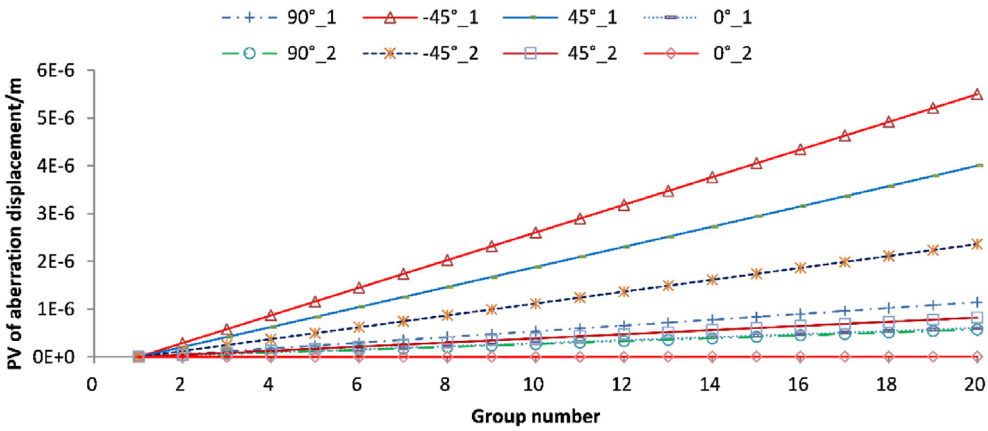

Fig. 5. Different ply thickness deviations applied to different ply angles and ply positions.

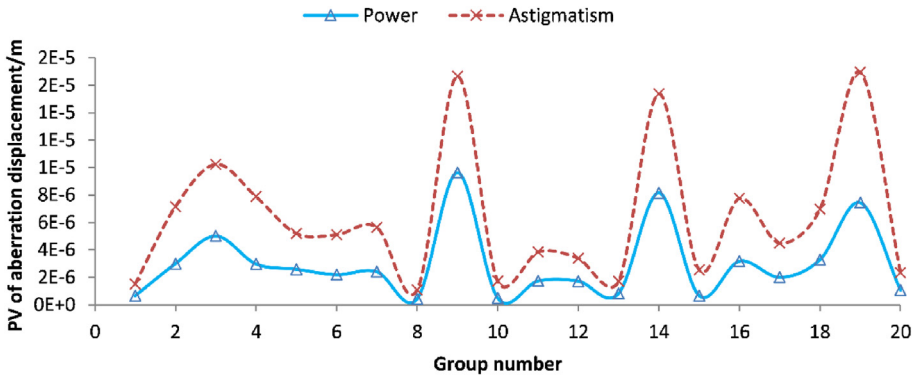

Fig. 6. Simulated results for power and astigmatic aberrations.

to weak for angles of −45°, 45°, 90°, and 0°. When the layup angle is constant, the sensitivity decreases as the distance from the middle plane decreases, because the moment increases as the distance from the middle plane increases with the same ply thickness deviation and in-plane force.

3.2.2. Relationship between ply angle misalignment and power and astigmatic aberrations

Similar to the procedures for the finite element computation of the ply angle misalignment, random variations in the thickness of the single-layer ply were generated, and the total thickness of the laminate was fixed. The 20 groups of random series generated using the Monte Carlo method were superimposed on the corresponding ply thickness. This provided the simulated variation in the CFRP laminate surface accuracy caused by the power and astigmatic aberrations, as shown in Fig. 6.

The simulation results show that ply thickness deviations cause power and astigmatic aberrations with similar trends. In addition, the astigmatic aberration is several times greater than the power aberration.

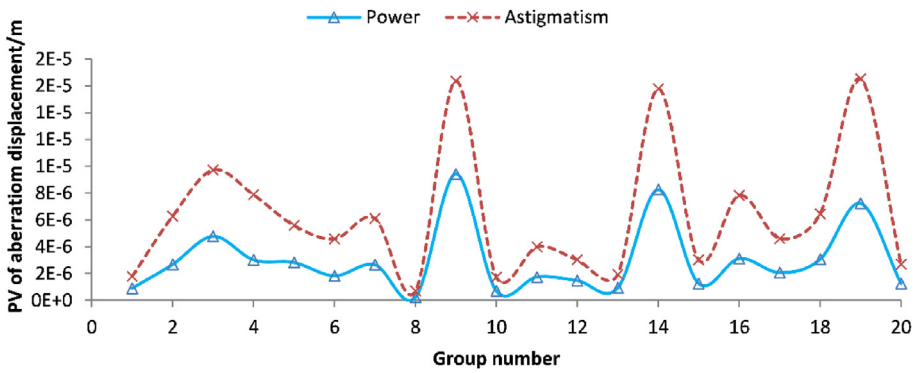

Fig. 7. Simulation results for power and astigmatic aberrations.

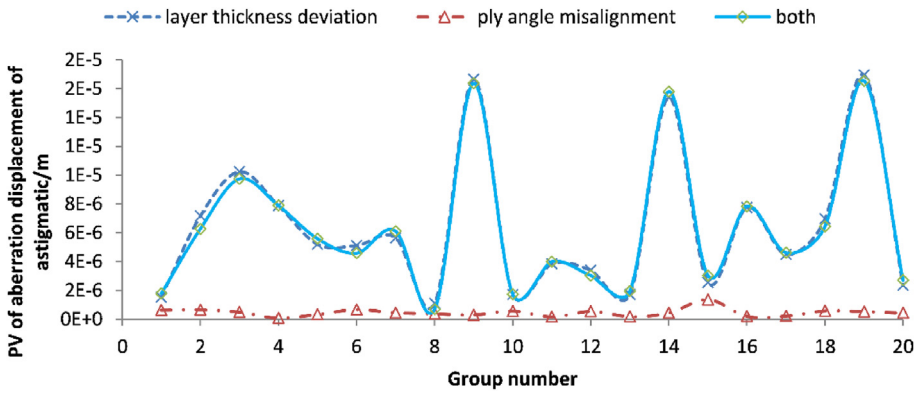

Fig. 8. Comparison of astigmatic aberration with and without the coupling effect.

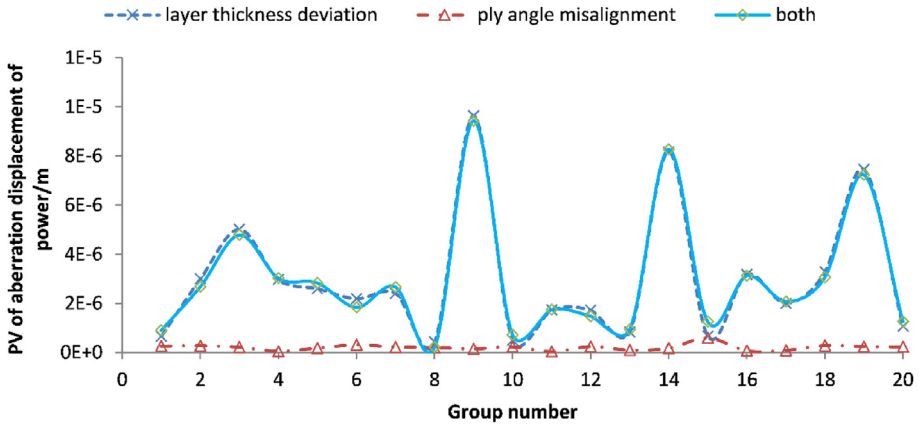

Fig. 9. Comparison of power aberration with and without the coupling effect.

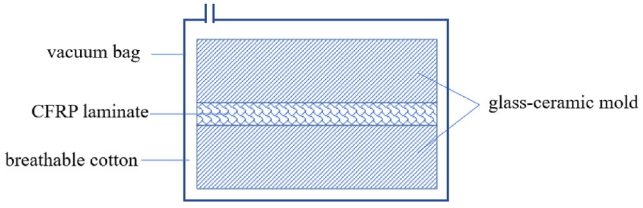

Fig. 10. Vacuum bag technology.

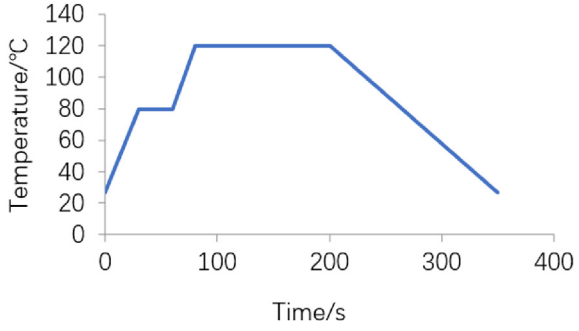

Fig. 11. Curing process parameters.

3.3. Simulation analysis of the relationship between the coupling effect and aberration

The numerical results obtained by applying the ply angle misalignments and ply thickness deviations obtained in Sections 3.1 and 3.2 are shown in Fig. 7.

The simulation results show that coupling of two factors do not produce a directly superimposed aberration. Instead, the two factors interact to affect the surface accuracy of CFRP laminates, as shown in Figs. 8 and 9.

4. Experimental analysis

In this section, the effects of ply angle misalignment and ply thickness deviation on the surface accuracy are verified through experimental analysis. Focus on the relationships between ply angle misalignment or ply thickness deviation and power or astigmatic aberration, and ply thickness deviations was measured.

4.1. Experimental scheme and surface result

Preparation technology of the laminate is vacuum bag technology in this study, as shown in Fig. 10. Curing process parameters is shown in Fig. 11. T700 unidirectional prepreg (produced by the Tianjin Onlytop Technology Company) was used for the experiments. The experimenters paved onto a 70 mm-diameter glass–ceramic mold with root

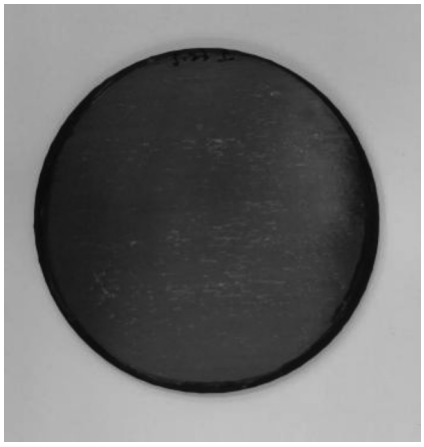

Fig. 12. Fabricated CFRP laminate.

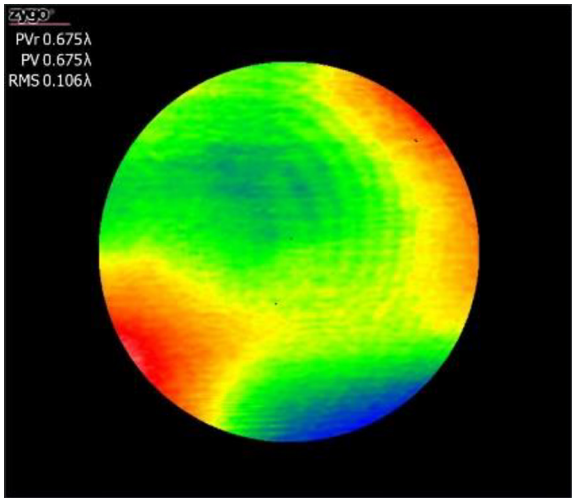

Fig. 13. Interferometer test result.

mean square (RMS) surface accuracy greater than $\lambda/40$ (λ = 632.8 nm) at an angle of $[90–45\ 45\ 0]_{2s}$. The other glass–ceramic mold with root mean square (RMS) surface accuracy greater than $\lambda/40$ (λ = 632.8 nm) are pressed on the CFRP laminate. Vacuum bags were made to solidify the model.

Considering the experimental operation and accuracy, several actions were taken to control the layup accuracy. First, the prepreg was cut into 250 × 250 mm squares, then it was paved on a 250 × 250 mm standard square model. Compared to the same operations with 70 × 70 mm squares, the larger size gave experimenters greater control over the ply angle misalignment, which could be reduced to ± 0.5° with the same paving length. To achieve this, the experimenters aligned one side of the prepreg with the standard point and limited the other side to ± 2.18 mm from the standard point. In comparison, this would be ± 0.61 mm for the 70 × 70 mm squares. Furthermore, the 250 × 250 mm squares could be paved more comfortably because twisting and adhesion may occur during pavement, and this is easier to control with the larger size.

A picture of the fabricated CFRP laminate is shown in Fig. 12. The interferometer test results are shown in Fig. 13.

During the experiment, three circular plates 70 mm in diameter were cut from the plate paved with 250 × 250 mm prepreg squares for each ply angle, then they were in a group. There were three groups: A, B, and C. This method meant that the ply angle misalignment of each group remained similar (ignoring twists in the carbon fibre). Twelve CFRP laminates were made in this experiment, and the surface results are listed in Table 3.

Astigmatic aberration and power aberration are two of the most important components of CFRP laminate surface accuracy aberration. Analysis of the test results in Fig. 14 and Table 4 show that power aberration can be controlled for a small order of magnitude, which only comprises approximately 5.6% of the entire surface aberrations. In contrast, astigmatic aberration forms a substantial part of the total aberrations, up to 96.6% at the peak. Therefore, the astigmatic aberration shows similar variations to the total surface aberration. When the surface accuracy deteriorates, the astigmatic aberration increases, and, correspondingly, the proportion of the total accuracy increases too. In conclusion, astigmatic aberration is the main factor limiting CFRP laminate surface accuracy.

4.2. Measurement of CFRP laminate ply thickness

The ply thickness at each angle in the CFRP laminates was measured using a REYENCE microscope. The laminate was cut to measure the thickness of each ply through the cross section. The ply angles of the CFRP laminate were $[90–45\ 45\ 0]_{2s}$, so an angle of –22.5° was selected for the cutting direction, as shown in Fig. 15. It was necessary to select an appropriate cutting direction to make the ply boundaries easier to distinguish, which reduces the risk of mismeasurement or immeasurability. For example, if the cutting direction was 90° (or 0°), it would have been difficult to distinguish the boundary between −45° and 45°, because the interval between the two angles and 90° (or 0°) would have the same cutting sections, making the measurement impossible. Similarly, if the cutting direction was 45° (or −45°), it would have been difficult to distinguish the boundary between 0° and 90°, because the intervals between the two angles and 45° (or −45°) would have the same cutting sections, making the measurement impossible. Therefore, the cutting direction could not be the angular bisector of adjacent angles. Because the laminate had a symmetric and balanced layup, both sides of the middle plane had the same angle 0° and there was no boundary, so they could be treated as a single ply during the measurement, with half the measurement result giving the thickness of a single-layer ply at 0°. This was equivalent because these

Table 3
Test results of the CFRP laminate surface (long wave band λ = 10.6 μm, in λ).

Number	Surface accuracy (RMS)	Power(RMS)	Astigmatic(RMS)	Without lower aberration (RMS)
A1	0.106	0.025	0.081	0.064
A2	0.105	0.014	0.085	0.060
A3	0.109	0.015	0.091	0.058
B1	0.402	0.028	0.393	0.076
B2	0.356	0.046	0.350	0.049
B3	0.483	0.076	0.474	0.042
C1	0.158	0.025	0.150	0.041
C2	0.185	0.033	0.173	0.058
C3	0.284	0.067	0.273	0.040

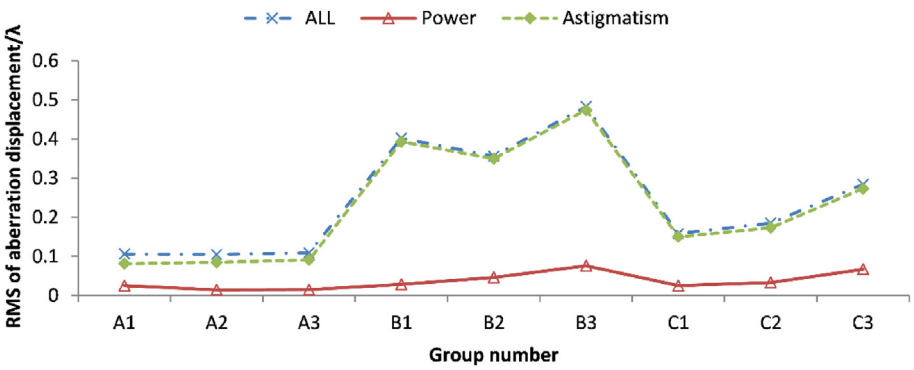

Fig. 14. Surface accuracy of different groups.

Table 4
Proportions of power and astigmatic aberrations.

Number	Power aberration proportion [%]	Astigmatic aberration proportion [%]
A1	5.6	58.8
A2	1.9	65.1
A3	1.8	69.7
B1	0.5	95.5
B2	1.7	96.6
B3	2.5	96.5
C1	2.5	90.0
C2	3.2	87.7
C3	5.6	92.5

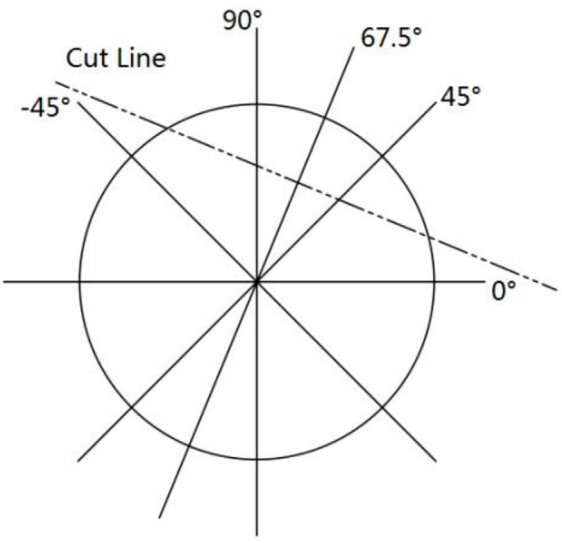

Fig. 15. CFRP laminate cutting line.

two plies had the same angle, they were both located in a symmetric position, and the floating property of the epoxy resin can be considered uniform at the macro scale.

The cut CFRP laminate areas tested are shown in Fig. 16. The substrates were cut with grinding wheels, and polished using 5000-mesh sandpaper to provide a smooth test surface.

The thickness of every ply was measured. An example of the measurements is shown in Fig. 17 and all of the results are shown in Tables 5 and 6. The laminate shown in Fig. 17 present an enormous porosity, the porosity affects the value of the thickness obtained in some degree. In this study we ignored it, take the average as the value.

Analysis of the data shows that ply thickness deviations were present. The mean value was 92.00 μm, and the standard deviation was approximately 9.074 μm. Based on the thickness measurement data, the effect of the thickness deviation on the CFRP laminate surface precision was analysed and the results are shown in Table 6.

From the simulation data, the nine samples in the experiment mainly showed astigmatic aberration caused by ply thickness deviation, as shown in Fig. 18. The power aberration was relatively small, which is consistent with the experimental results. However, there were some differences between the simulated and actual astigmatic aberrations, mainly because the simulation only accounted for the ply thickness deviation, without the ply angle misalignment which is difficult to measure accurately under currently available laboratory conditions. Moreover, there are other factors that cause astigmatic aberration, in addition to ply angle misalignment and ply thickness deviation. For example, the distortion and distribution consistency of the fibre bundles affects the symmetry of the plies and causes stretch–bending deformation of the laminates.

5. Conclusions

This study investigated the effects of ply angle misalignment and ply thickness deviation on the surface accuracy of CFRP laminates. It was shown theoretically, that in a pair of symmetric layers, these factors will generate moments that twist and deform the laminate, resulting in astigmatic aberrations in the surface accuracy. Subsequently, simulations were used to demonstrate that the effects of these factors are coupled to the laminate, which results in a nonlinear superimposition of the surface deformation. Finally, CFRP laminates with an average ply thickness of 92 μm and a standard deviation of ply thickness deviation of 9.074 μm were prepared for experimental analysis. The power aberrations on the surface were relatively small, while the astigmatic aberrations were dominant. The ply thickness deviation depends on many factors such as random distortion in the fibre tow, non-uniformity and randomness in the resin solidification, and uncertainty in the resin flow, so even though steps can be taken to reduce deviation, it is difficult to eliminate entirely. Due to the inevitability of ply angle misalignment and ply thickness deviation, it will be difficult to avoid astigmatic aberration on the surface of CFRP laminates produced using standard fabrication products entirely. Moreover, the test results are random due to the randomness of the two factors. This study only considered the effects of ply angle misalignment and ply thickness deviation in room temperature (It needs to be pointed out that the properties of laminates varied with the temperature), but there are other factors that affect the surface accuracy of CFRP laminates worthy of investigation.

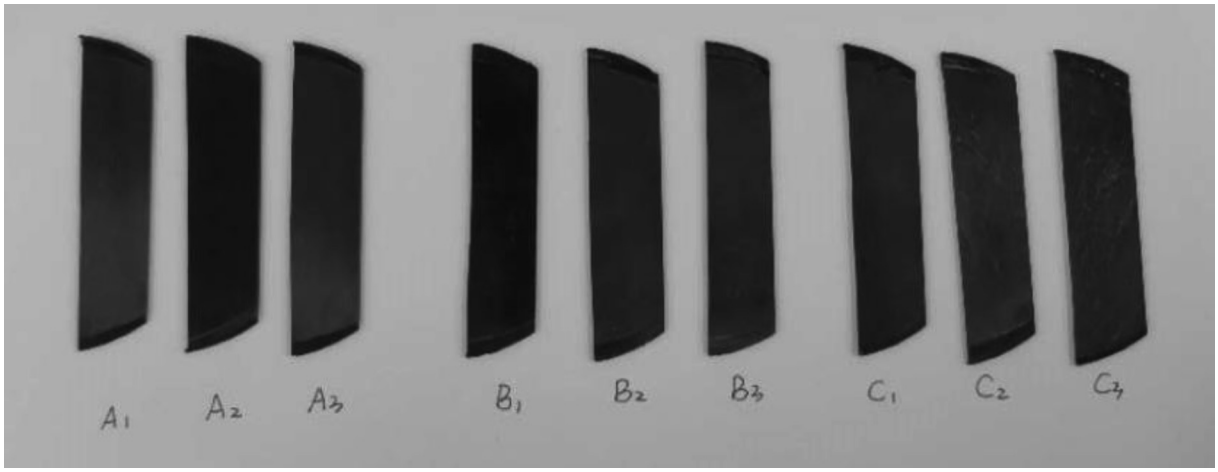

Fig. 16. Physical samples of the cut CFRP laminates.

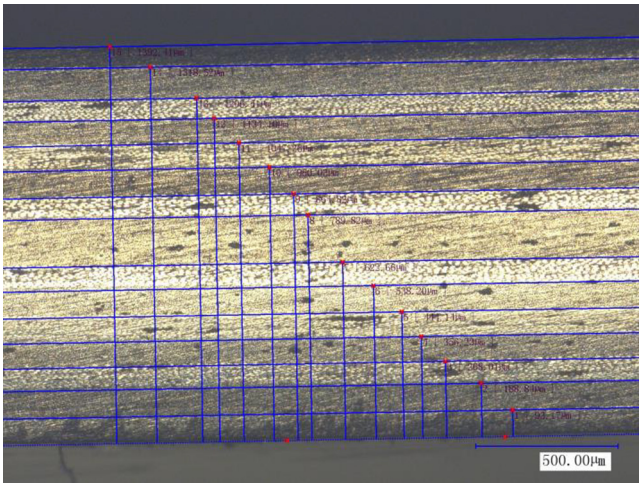

Fig. 17. Example of the measurement results.

Funding

This work was supported by the National Natural Science Foundation of China [grant number 51675506]; the Foundation for Excellent Young Scholars of Jilin Province, China [grant number 20190103015JH]; and the National Science and Technology Major Project of the Ministry of Science and Technology of China [grant number 2018YFF01011503].

CRediT authorship contribution statement

Luchao Cheng: Conceptualization, Methodology, Resources, Software, Writing - original draft. **Peng Gong:** Conceptualization, Methodology, Resources, Software, Writing - original draft, Supervision. **Qianglong Wang:** Resources, Software, Data curation. **Meng Zou:** Methodology, Resources. **Yaoyu Zhang:** Conceptualization, Methodology. **Zhenyu Liu:** Conceptualization, Methodology, Software, Funding acquisition, Writing - review & editing.

Table 5
Summary of CFRP laminate thickness measurement results (in μm).

Ply number	A1	A2	A3	B1	B2	B3	C1	C2	C3
1	88.43	93.17	73.2	98.73	94.02	97.09	96.92	104.28	86.68
2	94.11	95.67	90.03	87.04	82.9	87.89	88.99	83.14	89.48
3	92.67	79.17	102.79	85.75	96.72	92.84	91.78	94.15	86.67
4	90.02	88.22	103.92	88.54	85.6	100.87	101.81	98.18	110.45
5	89.97	87.91	85.8	117.87	102.98	91.69	103.2	95.4	86.68
6	80.05	93.88	98.39	81.46	101.34	73.48	94.87	99.53	88.08
7	85.73	84.64	76.34	80.01	89.02	91.35	91.21	89.82	96.46
8	100.135	83.58	101.995	89.825	91.84	115.89	91.1	80.5	72.7
9	100.135	83.58	101.995	89.825	91.84	115.89	91.1	80.5	72.7
10	85.76	75	109.51	84.4	116.92	86.27	87.68	88.29	89.48
11	95.65	95.21	97	84.24	84.08	94.13	91.88	84.3	96.46
12	103.88	87.23	101.14	84.24	91.55	85.13	100.33	102.41	95.07
13	88.45	86.84	89.95	106.67	94.33	79.63	104.2	99.51	92.27
14	102.37	72.41	84.23	94.08	97.14	103.84	94.88	99.47	79.69
15	89.79	112.01	98.41	74.76	97.76	80.03	90.4	94.05	89.48
16	99.81	73.89	95.52	74.87	88.41	108.74	103	91.19	85.28
Total thickness	1486.96	1392.41	1510.22	1422.31	1506.45	1504.76	1523.35	1484.72	1417.63

Table 6
Simulation results for the thickness deviation (in m).

	A1	A2	A3	B1	B2	B3	C1	C2	C3
Power	2.79E-07	3.89E-06	3.90E-06	3.03E-06	4.15E-07	5.51E-07	1.82E-07	9.34E-08	1.90E-06
Astigmatic	2.40E-06	9.85E-06	6.31E-06	7.27E-06	1.42E-06	2.13E-06	5.10E-07	7.48E-07	3.15E-06

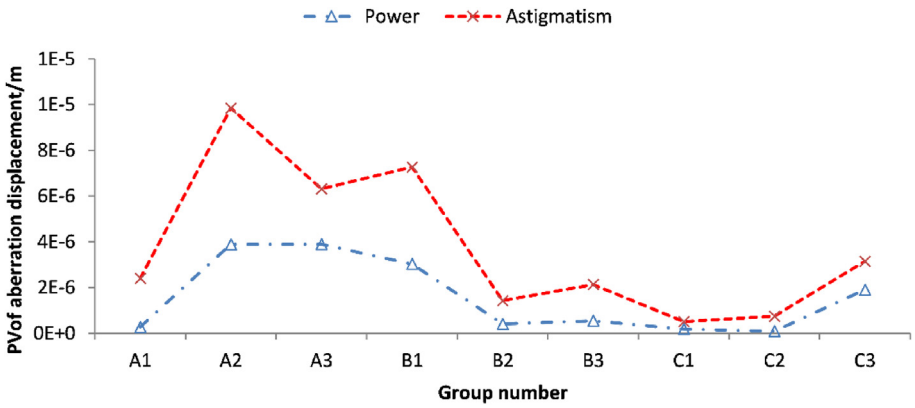

Fig. 18. Power and astigmatic aberrations caused by ply thickness deviation.

Declaration of Competing Interest

The authors declare that they have no known competing financial interests or personal relationships that could have appeared to influence the work reported in this paper.

References

[1] Galos J. Thin-ply composite laminates: a review. Compos. Struct. 2020;236:111920. https://doi.org/10.1016/j.compstruct.2020.111920.
[2] Awaki H, Oue C, Iwakiri H, Omatsu M, Yoshida T, Yokota T. Development of a lightweight x-ray mirror using thin carbon-fiber-reinforced plastic (CFRP). Sp. Telesc. Instrum. 2018 Ultrav. to Gamma Ray, vol. 10699, 2018, p. 106993R.
[3] Arao Y, Koyanagi J, Utsunomiya S, Kawada H. Analysis of thermal deformation on a honeycomb sandwich CFRP mirror. Mech. Adv. Mater. Struct. 2010;17:328–34.
[4] Sugita S, Awaki H, Kurihara D, Yoshioka K, Tomita Y, Ogi K, et al. Studies of lightweight x-ray telescope with CFRP. vol. 9144, SPIE; 2014, p. 914447.
[5] Steeves J, Pellegrino S. Ultra-thin highly deformable composite mirrors, 2013.
[6] Romeo RC, Martin RN. Progress in 1m-class lightweight CFRP composite mirrors for the ULTRA Telescope. In: Atad-Ettedgui E, Antebi J, Lemke D, editors. Optomech. Technol. Astron., vol. 6273, SPIE; 2006, p. 230–41.
[7] Wu KM, Avery BL. Fully isotropic laminates and quasi-homogeneous anisotropic laminates. J. Compos. Mater. 1992;26:2107–17.
[8] Vannucci P, Verchery G. A special class of uncoupled and quasi-homogeneous laminates. Compos. Sci. Technol. 2001;61:1465–73.
[9] Grédiac M. A procedure for designing laminated plates with required stiffness properties. application to thin quasi-isotropic quasi-homogeneous uncoupled laminates. J. Compos. Mater. 1999;33(20):1939–56.
[10] Yang Z, Zhang J, Xie Y, Zhang B, Sun B, Guo H. Influence of layup and curing on the surface accuracy in the manufacturing of carbon fiber reinforced polymer (CFRP) composite space mirrors. Appl. Compos. Mater. 2017;24:1447–58.
[11] Kulkarni P, Mali KD, Singh S. An overview of the formation of fibre waviness and its effect on the mechanical performance of fibre reinforced polymer composites. Compos. Part A Appl. Sci. Manuf. 2020;137:106013. https://doi.org/10.1016/j.compositesa.2020.106013.
[12] Arao Y, Koyanagi J, Utsunomiya S, Kawada H. Time-dependent out-of-plane deformation of UD-CFRP in humid environment. Compos. Sci. Technol. 2009;69:1720–5.
[13] Corrado A, Polini W. Analysis of process-induced deformation on the spring-in of carbon fiber-reinforced polymer thin laminates. J. Compos. Mater. 2019;53:2901–7.
[14] Hinckley M. Statistical evaluation of the variation in laminated composite properties resulting from ply misalignment. In: Breakwell JA, Genberg VL, Krumweide GC, editors. Adv. Opt. Struct. Syst., vol. 1303, SPIE; 1990, p. 497–511.
[15] Vincenti A, Vannucci P, Verchery G. Influence of orientation errors on quasi-homogeneity of composite laminates. Compos. Sci. Technol. 2003;63:739–49.
[16] Arao Y, Koyanagi J, Utsunomiya S, Kawada H. Effect of ply angle misalignment on out-of-plane deformation of symmetrical cross-ply CFRP laminates: Accuracy of the ply angle alignment. Compos. Struct. 2011;93:1225–30.
[17] Arao Y, Koyanagi J, Utsunomiya S, Kawada H. Analysis of thermal deformation on honeycomb sandwich CFRP mirror. Mech. Adv. Mater. Struct. 2010;17:328–34.
[18] Tanaka S, Ikeda T, Senba A. Sensitivity analysis of thermal deformation of CFRP laminate reflector due to fiber orientation error. J. Mech. Sci. Technol. 2016;30:4423–6.
[19] Thompson S, Bichon S, Grant R. Influence of ply misalignment on form error in the manufacturing of CFRP mirrors. Opt. Mater. Express 2014;4:79–91.
[20] Liu Q, Cai Y, Liu X, Yang Z, Jiang S, Leng S. Influence of the ply angle deviation on the out-of-plane deformation of the composite space mirror. Appl. Compos. Mater. 2019;26:897–911.
[21] Wilhelmsson D, Rikemanson D, Bru T, Asp LE. Compressive strength assessment of a CFRP aero-engine component – An approach based on measured fibre misalignment angles. Compos. Struct. 2020;233:111632.
[22] Steeves J, Pellegrino S. Post-cure shape errors of ultra-thin symmetric CFRP laminates: Effect of ply-level imperfections. Compos. Struct. 2017;164:237–47.
[23] Bosi F, Schlothauer A, Leclerc C, Pellegrino S. Cure-induced deformation of ultra-thin composite laminates. 2018 AIAA/ASCE/AHS/ASC Struct. Struct. Dyn. Mater. Conf., n.d.
[24] Tanaka S, Arai M, Goto K, Ikeda T. Quantitative investigations on the dimensional stability of a CFRP reflector model against temperature variations. Trans. Jpn. Soc. Aeronaut. Space Sci. 2019;62:275–83.
[25] Keith BD, Victor LG, Gregory JM. Integrated optomechanical analysis (second edition). SPIE press, 2012.